

Behavior of Castellated Steel Beams: State of the Art Review
Samadhan G. Morkhade, L. M. Gupta 39-48
PDF

Proposed SMA Tension Sling Damper for Passive Seismic Control of Building
S. H. Mehta, S. P. Purohit 49-59
PDF

Utilizing Steel Brace for Seismic Retrofitting of Old School Buildings with Open Ground Storey
T. Sharaf, O. M. Ramadan, S. Elsharly 60-70
PDF

The Effect of Plastic Hinge Location on the Flexural Strength Demand of Welded Flange Plate Connections
J. Kent Hsiao, S. Shrestha, V. R. R. Vootukuri, F. Mensah 71-84
PDF

Shear Strengthening of RC Beams Using NSM GFRP Bars or CFRP U-Wrap Sheets

# Seismic response control of modal building using shape memory alloy tension sling damper

Sujata H. Mehta and Sharadkumar P. Purohit*

Civil Engineering Department,
School of Engineering,
Institute of Technology,
Nirma University,
Ahmedabad, Gujarat, 382481, India
Email: 13extphde106@nirmauni.ac.in
Email: sharad.purohit@nirmauni.ac.in
*Corresponding author

**Abstract:** Unprestrained NiTinol shape memory alloy wire-based tension sling damper, SMA-TSD, is developed to produce passive damper force at ground story of a three-story modal building. Nonlinear hysteretic behaviour of superelastic SMA is represented by one-dimensional Tanaka model. SMA-TSD is characterised by linear Voigt model with equivalent stiffness and equivalent viscous damping components under seismic excitations to implement it with linear modal building. Equivalent viscous damping ratio is evaluated by proposed instantaneous damping approach more appropriately simulating practical scenario as well as constant damping approach used in other studies. Uncontrolled and controlled responses of modal building are obtained to prove efficacy of superelastic passive SMA-TSD. Seismic performance indices are found to reduce substantially for controlled modal building when design parameters of passive superelastic SMA-TSD are adjusted.

**Keywords:** tension sling damper; superelastic SMA; Tanaka model; modal building; performance indices.

**Reference** to this paper should be made as follows: Mehta, S.H. and Purohit, S.P. (2022) 'Seismic response control of modal building using shape memory alloy tension sling damper', *Structural Engineering*, Vol. 12, No. 3, pp.240–263.

**Biographical notes:** Sujata H. Mehta is a research scholar at Civil Engineering Department, School of Engineering, Institute of Technology, Nirma University, Ahmedabad, Gujarat, India. She received her Postgraduate degree from Gujarat University, Ahmedabad, Gujarat, India.

Sharadkumar P. Purohit is a Professor at Civil Engineering Department, School of Engineering, Institute of Technology, Nirma University, Ahmedabad, Gujarat, India. He received his Postgraduate and Doctoral degrees from Indian Institute of Technology Bombay (IITB), Powai, Mumbai, India. His research areas include dynamic response control of structures, reduced and large scale experimental investigation on structural element/structure, seismic analysis and design of structures, smart materials application to civil structures, experimental investigation on composite steel-concrete sections. He is involved in externally funded research projects in these research areas. He is teaching structural engineering related courses to undergraduate and postgraduate program.

## 1 Introduction

Seismic response control of buildings can be achieved by modifying rigidities, masses, damping, shape, and by providing passive or active counter forces. Practical difficulties in modifying mass, shape and rigidity have led to evolution of base isolation technique and provision of counter forces through passive and active dampers (Tsai and Kelly, 1994; Soong and Constantinou, 1994). Passive dampers absorb the seismic energy and reduce seismic response of building without any external power input while active dampers need external power supply and can vary the counter force as per requirement. However, active dampers may not remain functional due to power disruption during seismic event and may destabilise system under powerful excitation. Passive dampers are found to be safe, reliable and reusable for seismic applications. Passive dampers like metallic yield damper, friction damper, viscoelastic damper, viscous damper, etc. perform well under seismic excitations (Symans et al., 2008). Efficacy of such dampers and base isolator for framed buildings for near-fault and far-fault seismic excitations have been studied with more emphasis on near-fault seismic excitations comprising of impulsive type accelerograms, which show large-amplitude pulses (Foti, 2014). In recent past, dampers have been developed utilising materials with controllable properties, called smart materials, such as piezo-electric, electro-rheological fluid, magneto-rheological fluid, etc. (Dyke et al., 1996; Jansen and Dyke, 1999; Xu et al., 2000; Soong and Spencer, 2002). Understanding of unique characteristics of smart materials through experimental research has encouraged their use as a damper with improved properties as compared to passive damper for seismic response control of buildings and structures. Variety of semi-active and active dampers with various control algorithms have been successfully implemented for seismic response control of structural frames (Spencer and Nagarajaiah, 2003; Dyke and Jansen, 1999; Purohit and Chandiramani, 2010; Lavasani and Doroudi, 2020).

A relatively newer class of smart materials having unique characteristics of shape memory effect (SME) and superelasticity, named shape memory alloys (SMA) have been commercially explored and implemented exceedingly in the domain of biomedical, aeronautical, robotics and automotive industry (Buehler and Wiley, 1961; Jani et al., 2014). SMA exhibit non-linear hysteresis, high actuation stress and strain, high energy density and three dimensional actuation other than its' unique characteristics making it suitable for civil engineering applications (Jani et al., 2014). While Cu-Zn, Cu-Al and Cu-Sn based SMAs have shortcomings of thermal stability, brittleness and mechanical strength, NiTi alloys are widely used SMAs for engineering applications (Dasgupta, 2014). Further, alloy composition and properties of SMA wire are found to have considerable effect on its capabilities to improve structural response (Hartl and Lagoudas, 2008). Clarke et al. (1995) and Ocel (2004) experimentally established effectiveness of NiTi wires with steel framed structures. SMA have been used for shape restoration, self-rehabilitation, seismic retrofit of structural elements, base isolation, energy dissipation, etc. as a part of civil engineering applications (Song et al., 2006). Huang et al. (2014) and Ghodke and Jangid (2016) have implemented SMA as components of base isolator. Dolce et al. (2005) and McCormik et al. (2006) have implemented SMA based passive damper with reinforced concrete frame. SMA based passive damper has been used for seismic response control of steel frame by Mortazavi et al. (2013) and SMA based BRBs have been developed by Miller et al. (2012). Due to high damping capacity, greater fatigue life and large recoverable strains, NiTi wires are increasingly

studied for structural response control (Ren et al., 2007; Fan et al., 2019). Zhang and Zhu (2007) have also established that NiTinol wire having 0.6 mm diameter can sustain 2000 load cycles with maximum strain amplitude of 8%. It was found that prestrained NiTi wires were more effective in controlling norm drift ratio and norm level acceleration of a building while unprestrained wire were more effective in controlling residual drift (Zhang and Zhu, 2008).

Since most of civil engineering applications of SMA, hitherto, rely on prestraining to improve damping characteristics of the dynamic system, the major objective of the present paper is to utilise hysteretic properties of superelastic SMA, without prestraining, for seismic response control of modal building. It is further aimed to develop novel tension only damper using superelastic SMA wires and implement it for passive seismic response control of modal building. In the present paper, novel SMA based tension sling damper (SMA-TSD) is developed and is fitted between ground and first story of three story modal building. SMA-TSD utilises unprestrained NiTi based SMA wire with superelastic properties to improve damping characteristic of the building. Hysteretic stress strain relationship of SMA-TSD is represented by one-dimensional unified Tanaka model. It is implemented with linear modal building under seismic excitations using linear Voigt model comprising of stiffness and damping components following seismic guidelines of AASHTO – guide specification for seismic isolation design (AASHTO, 2014). Performance of SMA-TSD under pulse and strong motion type of seismic excitations is studied using more practical instantaneous damping approach proposed in the present study along with constant damping approach used in other studies. Suitable design parameters such as numbers, diameter and length of SMA sling are evaluated in order to ensure peak strain in SMA to remain within elastic recoverable limit of~4% to 6%. Peak response quantities of the modal building controlled by SMA-TSD are compared with results reported by Dyke et al. (1996), using controllable fluid based magnetorheological (MR) damper to establish its' efficacy.

## 2 SMA based tension sling damper

SMA-TSD employing unprestrained superelastic NiTi wires is developed to produce passive damping force. Geometric design of the damper is so proposed that SMA slings are subjected to tensile strain under alternative input motion from the source. Experimental studies have established that damping offered by SMA based dampers is a function of wire diameter, mechanical properties, strain rate and amplitude, prestaining of SMA wire and ambient temperatures (Hartl and Lagoudas, 2008). Design parameters of the unprestrained superelastic SMA-TSD considered for the present study are diameter and length of SMA wire at ambient temperature. These design parameters of the damper fitted with different structures should be estimated constraining maximum recoverable elastic strain of~4%–6%.

Isometric view of the SMA-TSD is shown in Figure 1 with various components, where number and diameter of superelastic NiTi SMA slings may vary as per damper design. Bottom plate with slit has two fixed rods connected on either side of the rigid core box. Bottom plates are connected to the fixed bracing element as shown in Figure 2(a) and plan view of SMA-TSD at rest is shown in Figure 2(b). Set of SMA slings are wound around fixed rods on either side of the rigid core box. Rigid core box receives input motion through central rigid rod connected to top plate, causing tensile

strain in one set of SMA slings at a time while other set of SMA slings on opposite side of rigid core box disengages itself until velocity of SMA-TSD is ceased. Figure 2(c) and Figure 2(d) show motion of SMA-TSD fitted with modal building when subjected to seismic excitations and corresponding set of engaged SMA slings producing passive damper force. Upon reversal of input motion, set of SMA slings will regain original state due to superelasticity. Placement of SMA-TSD in principal diagonal is preferred over horizontal position attributed to flexibility of accommodating relatively longer design length of SMA tension slings.

**Figure 1** SMA based tension sling damper (SMA-TSD) – 3D view (see online version for colours)

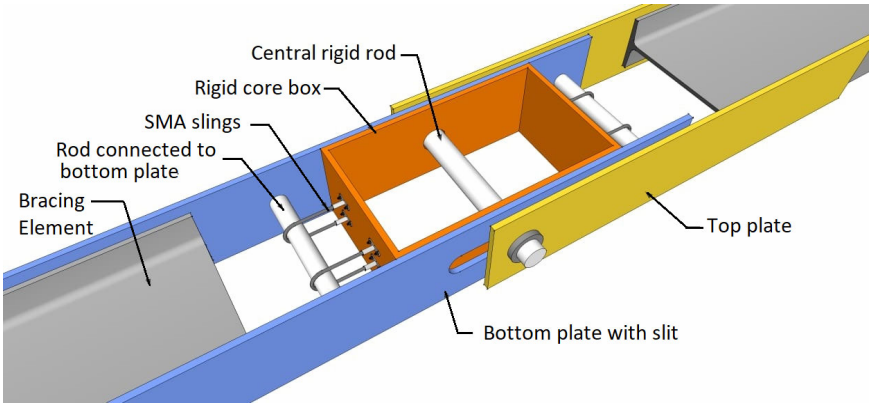


**Figure 2** (a) SMA-TSD fitted in principal diagonal of three story benchmark building (b) SMA-TSD at rest (c) right sway of SMA-TSD and (d) left sway of SMA-TSD under input motion (see online version for colours)

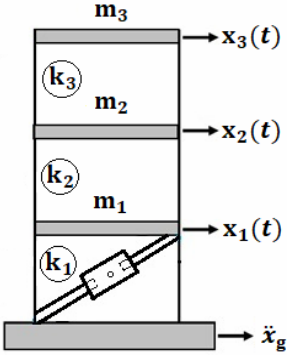


(a)

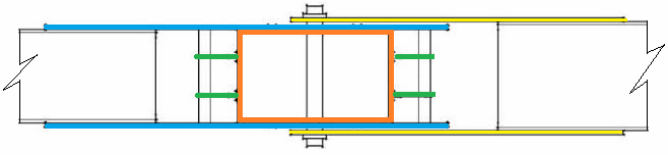

(b)

**Figure 2** (a) SMA-TSD fitted in principal diagonal of three story benchmark building (b) SMA-TSD at rest (c) right sway of SMA-TSD and (d) left sway of SMA-TSD under input motion (continued) (see online version for colours)

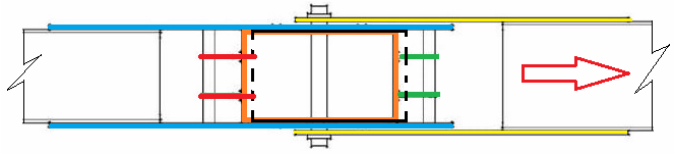

(c)

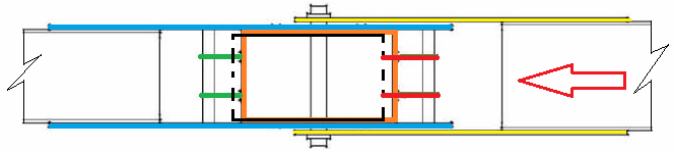

(d)

SMA-TSD developed in the present study has few distinct advantages when compared with currently practiced passive devices like steel X-bracings, Pall friction damper, SMA wire bracings and buckling restrained bracings (BRBs) which include:

1 elimination of buckling of SMA-TSD due to absence of compressive force in the damper

2 saving of SMA material as the component carrying compressive force is eliminated

3 recentering of structural system without any residual displacement

4 flexibility to adjust design parameters to meet passive force requirements to varied input motion

5 reusability and reconfigurability.

Present study aims to establish efficacy of developed SMA-TSD when used passively vis-à-vis passive off MR damper device used by Dyke et al. (1996), with three story modal building.

## *2.1 Hysteresis model of SMA-TSD*

SMA are alloys which have ability to undergo large deformation and return to their undeformed shape upon removal of the stress due to superelastic effect. Out of various types of SMA like Cu based SMAs, NiTi SMAs, ferrous SMAs, shape memory ceramics and shape memory polymers; NiTi based SMAs are most preferred in engineering applications because of its superior ductility and high fatigue life. NiTi alloys were discovered by William Buehler in 1959 but its commercial applications became possible after shape memory effect was revealed by William Buehler and Frederick Wang in 1962. Present study uses NiTinol SMA with 55% Nickel and 45% titanium. Study of SMA hysteretic behaviour is very important to effectively utilise SMA-TSD with modal building under various seismic excitations. However, it is difficult to establish a constitutive model which is appropriate for the design of SMA device due to complexity of the SMA material behaviour (Ren et al., 2007).

Tanaka (1990) has developed a one-dimensional phenomenological model for SMA that uses volume fraction of martensite as an internal variable and defines strain as a function of stress and temperature. The model provides set of exponential equations for evolution of kinematics of martensite volume fraction for SMA. Tanaka's model was extended by Liang and Rogers (1997) by describing the transformation kinetics through cosine law in place of exponential function. Brinson (1993) has improved the thermo-mechanic constitutive relationship to represent SMAs behaviour over the full range of temperature. Graesser and Cozzarelli (1991) have studied macroscopic characteristics of SMA and modified existing one dimensional hysteresis model by Ozdemir (1976) which is a special case of Bouc-Wen model. This is widely known as classical G-C model, has considered varying levels of strain amplitude and strain rate for the cyclic behaviour of NiTi SMAs. Wilde et al. (1998) have extended classical G-C model to include hardening behaviour of SMA materials. G-C model uses identical parameters for loading and unloading boundaries leading to some difference between prediction and experimental results and thus model is updated by Ren et al. (2007) by different parameters for loading and unloading branches. These one dimensional rate dependent models are computationally intensive by its formulation. In the present study, hysteretic behaviour of SMA is represented by Tanaka's one-dimensional phenomenological model due to its simplicity and versatility.

**Table 1** Mechanical properties of NiTinol SMA wire

| | |
|---|---|
| Modulus of elasticity for martensite and austenite, $E_M$ and $E_A$ | 46 GPa and 55 GPa |
| Austenite and martensite start temperature, $A_S$ and $M_S$ | –3°C and –28°C |
| Austenite and martensite finish temperature, $A_f$ and $M_f$ | 7°C and –43°C |
| Stress influence co-efficient, $C_A = C_M$ | 7.4 MPa/°C |
| $H^{cur} = H^{max}$ | 0.0560 |

Tanaka model employed in present study to represent hysteretic behaviour of SMA does not allow explicit inclusion of loading rate. Experimental studies carried out by Ren et al. (2007) on NiTinol SMA wire with different strain rates suggested increase in dissipated energy for increment of strain rate in the range of 3 mm/min to 15 mm/min, however, amount of dissipated energy reduces for strain rate beyond 15 mm/min. This finding is consistent with similar studies conducted by Toboushi et al. (1998) and Fan et al. (2019). The largest value of RMS strain rate experienced by the NiTinol wire in the present study, is 6.6 mm/min due to various seismic excitations. Hysteretic characteristics of the NiTinol SMA wire are considered for strain rate 3 mm/min in the present study, projecting reduced dissipated energy as compared to the expected amount of dissipated energy at actual strain rates. Thus, seismic response control by developed passive SMA-TSD leads to conservative results. This may be sufficient to establish a proof of concept for passive superelastic SMA-TSD for seismic response control of the modal building. Table 1 shows mechanical properties of NiTinol SMA wire considered in the present study (Hartl and Lagoudas, 2008).

Hysteretic behaviour of NiTinol wire used in passive SMA-TSD is represented by unified one dimensional Tanaka model for isothermal process as,

$$\sigma = \left[E_A + \xi\left(E_M - E_A\right)\right]\left[\varepsilon - \xi H^{cur}(\sigma)\right] \tag{1}$$

where ξ = % of martensite by volume fraction and $H^{cur}$ ($\sigma$) = maximum transformation strain, $E_A$ = elastic modulus of austenite, $E_M$ = elastic modulus of martensite, $\sigma$ = mechanical stress and $\varepsilon$ = total strain in SMA wire.

Loading/unloading of set of NiTinol SMA tension slings of passive SMA-TSD induces phase transformation represented by percentage of martensite by volume fraction '$\xi$', which is a function of applied stress. Martensite volume fraction ($\xi$) can be evaluated through equation (2) to equation (5).

$$\xi = 0; \qquad \text{if } T \geq M_s^{\sigma} \text{ or } T \geq A_f^{\sigma} \tag{2}$$

$$\xi = \frac{\left(M_s^{\sigma} - T\right)}{\left(M_s - M_f\right)}; \qquad \text{if } M_f^{\sigma} < T < M_s^{\sigma} \tag{3}$$

$$\xi = \frac{\left(A_f^{\sigma} - T\right)}{\left(A_f - A_s\right)}; \qquad \text{if } A_s^{\sigma} < T < A_f^{\sigma} \tag{4}$$

$$\xi = 1; \qquad \text{if } T \leq M_f^{\sigma} \text{ or } T \leq A_s^{\sigma} \tag{5}$$

where

$$A_s^{\sigma} = A_s + \frac{\sigma}{C_A}; \qquad M_s^{\sigma} = M_s + \frac{\sigma}{C_M};$$

## *2.2 Characterisation of passive SMA-TSD*

Implementation of Tanaka model representing nonlinear hysteresis behaviour of SMA-TSD with linear modal building requires tedious and computationally intensive nonlinear dynamic analysis to be performed. Most research studies on nonlinear hysteresis passive damping devices utilise various linear models developed over a period of time for their simplified implementation with linear systems. Various seismic codes like AASHTO, permits modelling of nonlinear hysteretic material with equivalent linear elastic stiffness and equivalent viscous damping. AASHTO guide specifications for seismic isolation design allows such modelling of nonlinear base isolators for its' preliminary design. It further specifies applicability of equivalent elastic stiffness and viscous damping ratio modelling if equivalent viscous damping ratio derived does not exceed by 30%. This modelling approach has been implemented in isolator for seismic response control of unsymmetrical building and exhibited promising results (Ghodke and Jangid, 2016). This approach yields good estimate of peak displacement of base isolator and are found suitable for flexible structures (Sodha et al., 2021). NiTinol SMA wire used in passive SMA-TSD is considered as viscoelastic material in the present study since its behaviour depends not only on current loading condition but on the loading history (Sun and Lu, 1995). The viscoelastic material is well defined by Voigt model which is a combination of a linear spring and a dashpot. The force and displacement relationship of Voigt model for linear theory is given by

$$F(t) = kx(t) + c\dot{x}(t) \tag{6}$$

where $k$ is stiffness of the material, $c$ is damping of the material, $x$ and $\dot{x}$ are displacement and velocity of the input motion.

Nonlinear hysteresis behaviour of passive SMA-TSD can be characterised as linear Voigt model in which stiffness, $k$, and damping, $c$, of equation (6) are replaced with equivalent stiffness $k_{eq}$, and equivalent linear viscous damping $c_{eq}$, to be derived from flag shaped nonlinear hysteresis stress-strain curve given by Tanaka model. The modified force-displacement relationship of linear Voigt model given by equation (7) is termed as equivalent linear viscoelastic model of passive SMA-TSD.

$$F_{SMA}(t) = k_{eq}x(t) + c_{eq}\dot{x}(t) \tag{7}$$

Figure 3 shows hysteresis curve of NiTinol SMA super-imposed with equivalent viscoelastic model to define equivalent linear parameters of equation (7). Equivalent stiffness, $k_{eq}$, can be determined as follows,

$$k_{eq} = \frac{\left(F_{\max} - F_{\min}\right)}{\left(x_{\max} - x_{\min}\right)} \tag{8}$$

where $F_{max}$ and $F_{min}$ are maximum and minimum force induced by passive SMA-TSD, $x_{max}$ and $x_{min}$ are maximum and minimum displacement of passive SMA-TSD.

The equivalent viscous damping, $c_{eq}$, expresses energy dissipation capacity of the material during vibration, as

$$c_{eq} = 2\xi_{eq}\sqrt{k_{eq}m} \tag{9}$$

where $\xi_{eq}$ is the equivalent viscous damping ratio and $m$ is mass of the story where SMA-TSD is fitted. Equivalent viscous damping ratio $\xi_{eq}$, can be defined following energy dissipation by SMA-TSD in one cycle as

$$\xi_{eq} = \frac{W_D}{2\Pi k_{eq}x_{\max}^2} \tag{10}$$

where $W_D$ is energy loss per cycle by the hysteretic SMA-TSD. The energy loss per cycle within the flag-shaped hysteresis loop of SMA is determined from area covered from the hysteresis loop from known coordinates of SMA NiTinol wire at ambient temperature.

Damping force given by equation. (7) for SMA-TSD in the present paper is estimated by following two approaches;

1 Instantaneous damping approach: In this approach equivalent linear parameter for damping, $c_{eq}$, is evaluated at each instant of time from hysteretic force-displacement curve as it grows with input motion. The proposed approach is simulating more closely practical situation of damper force generation by passive SMA-TSD.

2 Constant damping approach: In this approach equivalent linear parameter for damping, $c_{eq}$, is determined equating energy dissipated per cycle by hysteresis force-displacement curve with viscous damping curve as shown in Figure 3 which remains constant irrespective of input motion.

This approach is used by few studies for structural response control of system under dynamic excitation with SMA-based devices. One of the recent works by Ghodke and Jangid (2016) represented non-linear SMA hysteresis model by Ren et al. (2007), with equivalent linear elastic viscous model for base isolated benchmark building following AASHTO guidelines on hysteretic device. Representing hysteretic passive damper device

by linear viscoelastic model was found compatible for preliminary design of the device. It has been found that it conservatively predicts displacement and base shear while underpredicts floor acceleration (Sodha et al., 2021). However, exploring use of linear viscoelastic model representing variety of nonlinear hysteretic energy dissipation devices is essential to prove its' capability to capture structural response close to corresponding nonlinear hysteretic model. AASHTO guide specifications for seismic isolation design permits use of linear viscoelastic model for nonlinear hysteretic damping curve if equivalent viscous damping ratio is up to 30%.

**Figure 3** Hysteresis curve of SMA NiTinol wire and its equivalent linear model (see online version for colours)

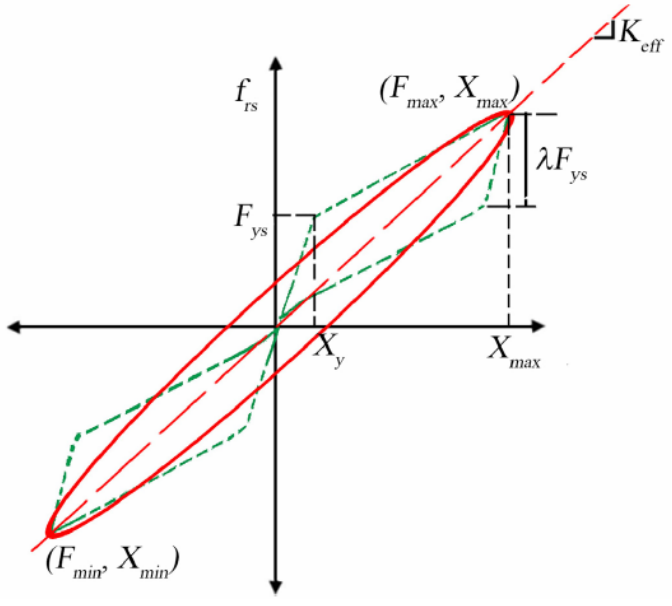


*Source:* Ghodke and Jangid (2016)

The hysteresis behaviour of SMA-TSD represented by unified Tanaka model subjected to seismic excitations have been evaluated and representative plot for Kobe seismic excitation is given in Figure 4(a). SMA-TSD is characterised as equivalent linear viscoelastic model following concept stated in Figure 3 and using equation (7) to equation (10) with instantaneous damping approach. Figure 4(b) shows damper force to damper displacement relationship derived through equivalent linear viscoelastic model. It is evident that peak damper force and peak displacement obtained by equivalent linear viscoelastic model, Figure 4(b), shows good agreement with corresponding values by Tanaka model, Figure 4(a).

Damper force to damper displacement for SMA-TSD is determined considering linear viscoelastic model with constant damping approach under Kobe seismic excitations and as shown in Figure 4(c). This approach also shows good agreement for peak damper force and peak displacement values with Tanaka model, Figure 4(a). Energy dissipated by SMA-TSD defined by unified Tanaka model is calculated as 4.56 J while it is 4.75 J for equivalent viscoelastic model with constant damping approach where damper mass is assumed to be in the range of 10 kg to 12 kg. SMA-TSD characterised as linear

viscoelastic model and fitted to modal building is solved considering both, instantaneous damping approach and constant damping approach discussed above, neglecting mass of the damper since it is very less (~4% of total mass of the modal building).

**Figure 4** (a) Damper force vs. damper displacement of SMA-TSD by Tanaka model for Kobe seismic excitation (b) Damper force vs. damper displacement of SMA-TSD by equivalent viscoelastic model with instantaneous damping approach for Kobe seismic excitation (c) Damper force vs. damper displacement for SMA-TSD by equivalent viscoelastic model with constant damping approach for Kobe seismic excitation

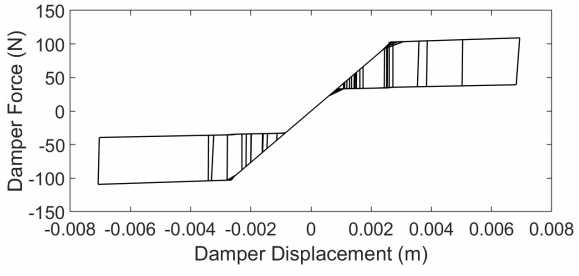


(a)

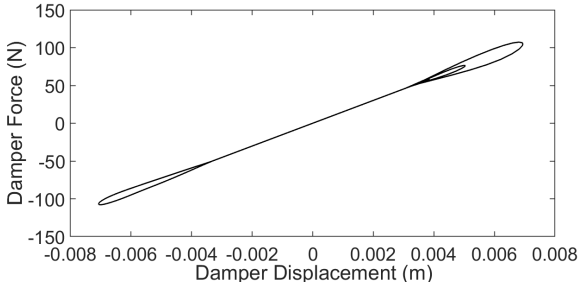


(b)

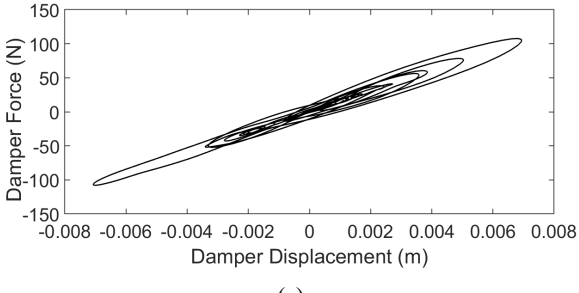


(c)

## 3 Modal building fitted with SMA-TSD

Building considered in the study is a laboratory based modal building by Dyke et al. (1996) widely used to test efficacy of control devices developed by researchers. Three story modal building fitted with SMA-TSD in principal diagonal at the ground story is shown in Figure 2(a). A lumped mass modelling approach is used to derive equation of

motion for modal building. Equation of motion for a controlled modal building with SMA-TSD is given as

$$M\ddot{x}(t) + C\dot{x}(t) + Kx(t) = Gf(t) - ML\ddot{x}_g(t) \tag{11}$$

where $M$ = mass matrix, $C$ = damping matrix, $K$ = orthogonal stiffness matrix, $G$ = location of SMA-TSD, $f(t)$ = passive SMA-TSD force, $L$ is influence vector associated with seismic ground excitation, $x(t)$, $\dot{x}(t)$ and $\ddot{x}(t)$ are displacement, velocity and acceleration vectors of the mass relative to the ground. Mass, stiffness and damping matrices are given by equation (12) as defined by Dyke et al. (1996).

$$\begin{aligned} M &= \begin{bmatrix} 98.3 & 0 & 0 \\ 0 & 98.3 & 0 \\ 0 & 0 & 98.3 \end{bmatrix} kg; \qquad K = 1\times10^5 \begin{bmatrix} 12 & -6.84 & 0 \\ -6.84 & 13.7 & -6.84 \\ 0 & -6.84 & 6.84 \end{bmatrix} N/m; \\ C &= \begin{bmatrix} 175 & -50 & 0 \\ -50 & 100 & -50 \\ 0 & -50 & 50 \end{bmatrix} Ns/m; \; f = \left[F_{SMA}\right]; \quad G = \begin{bmatrix} -1 \\ 0 \\ 0 \end{bmatrix}; \quad L = \begin{bmatrix} 1 \\ 1 \\ 1 \end{bmatrix}; \end{aligned} \tag{12}$$

Passive damping force by SMA-TSD and its location are defined in equation (12). Influence vector, $L$, indicating location of masses for the modal building is also defined in equation (12). Displacement degree of freedom $x = [x_1\ x_2\ x_3]^T$ associated with mass, $m_i$, where $i$ = 1,2,3 are defined as shown in Figure 2a.

Defining state $z$ vector, $z = [\ x\ \ \dot{x}\ ]^T$ and output vector $y = \left[\ddot{x}_1 \quad \ddot{x}_2 \quad \ddot{x}_3 \quad x_1 \quad x_2 \quad x_3\right]^T$, equation (11) can be converted to state space form given by,

$$\dot{z} = Az + Bf + E\ddot{x}_g \tag{13}$$

$$y = Cz + Df \tag{14}$$

where $A$ is system matrix, $B$ is input matrix, $C$ is output matrix, $D$ is direct transmission matrix and $E$ is location matrix of seismic ground excitation.

$$\begin{aligned} A &= \begin{bmatrix} 0 & I \\ -M^{-1}K & -M^{-1}C \end{bmatrix}; \quad B = \begin{bmatrix} 0 \\ M^{-1}G \end{bmatrix}; \quad E = -\begin{bmatrix} 0 \\ L \end{bmatrix}; \\ C &= \begin{bmatrix} -M^{-1}K & -M^{-1}C \\ I & 0 \end{bmatrix}; \quad D = \begin{bmatrix} M^{-1}G \\ 0 \end{bmatrix} \end{aligned} \tag{15}$$

In the present study, Modal building is subjected to two types of seismic ground excitations; pulse type – Kobe and Lomaprieta; strong motion type – El Centro and Taft seismic ground excitations for comparison and adding dataset to existing literature. Seismological details of these seismic ground excitations are given in Table 2. Equation (11) to equation (15) are solved using 4$^{th}$ order Rangekutta numerical integration method with MATLAB based programming considering both approaches to estimate equivalent linear damping, $c_{eq}$, for SMA-TSD as defined in Section 2.2.

**Table 2** Seismological details of pulse and strong motion type seismic ground excitations

| *Seismic excitation* | *Fault and component* | *D (km)* | *Scale* | | *Data points* | *Δt (s)* | *PGA (m/s²)* |
|---|---|---|---|---|---|---|---|
| | | | *M* | *MMI* | | | |
| Kobe (1995) – KJMA station | Strike-slip N-S | 1.0 | 6.9 | X | 2,400 | 0.02 | 8,132 (0.83g) |
| Lomaprieta (1989)-Corralitos station | Oblique slip (reverse) E-W | 2.8 | 7.0 | IX | 7,985 | 0.005 | 6,278 (0.64g) |
| El Centro (1940) imperial valley irrigation district – array station 09 | Strike-slip N-S | 12.2 | 6.9 | X | 1,500 | 0.02 | 2,845 (0.29g) |
| Taft (1952) Lincoln school station | Oblique slip E-W | 36.2 | 7.3 | XI | 3,400 | 0.02 | 1,756 (0.17g) |

Notes: D – distance from fault, M – magnitude, MMI – modified Mercalli scale intensity, Δt – acceleration recording interval, PGA – peak ground acceleration.

Seismic response of modal building fitted with SMA-TSD is evaluated in terms of normalised performance indices (PI) defined by Ohtori et al. (2004). Relevant PI's considered in the present study are peak interstory drift ratio $J_1$, level acceleration $J_2$, base shear $J_3$ and control force $J_{11}$ as shown in equation (16).

$$J_1 = max\left(\frac{\max\left(\left(\left|\frac{d_i(t)}{h_i}\right|\right)\right)}{\delta^{max}}\right); \qquad J_2 = max\left(\frac{\max|\ddot{x}_{ai}(t)|}{\ddot{x}_{ai}^{max}}\right);$$
$$J_3 = max\left\{\frac{|\max|\sum_i m_i\ddot{x}_{ai}(t)}{F_b^{max}}\right\}; \qquad J_{11} = max\left\{\frac{\max|f_l(t)|}{W}\right\}; \tag{16}$$

where, $d_i$ (t) is interstory drift and $h_i$ is the height of the of controlled modal building, $\delta^{max}$ is maximum uncontrolled interstory drift, $\ddot{x}_{ai}(t)$ and $\ddot{x}_{ai}^{max}$ are absolute acceleration for controlled and uncontrolled buildings, respectively. $m_i$ is seismic mass of the story here $i$ = 1,2,3, $F_b^{max}$ is maximum uncontrolled base shear, $f_l$ ($t$) is control force offered by SMA-TSD and W is the total seismic weight of the modal building.

## 4 Results and discussion

Controlled modal building fitted with SMA-TSD and uncontrolled modal building, $F_{SMA}$ = 0 in equation (11), have been solved under pulse and strong motion type seismic excitations. Pulse type seismic excitations comprises of severe acceleration pulses for shorter duration while strong ground motion type seismic excitation contain significant acceleration over longer time duration.

Modal building being a scaled laboratory-based model, seismic excitation data has been scaled down by five times the recorded rate except for Lomaprieta seismic excitation, where data was already available at the required record rate. It has been verified that these seismic excitations are capable to excite the fundamental modes of vibration of the modal building. Uncontrolled seismic response of the modal building has been obtained in terms of peak values of displacement, interstory drift and acceleration for El Centro seismic excitations and are reported in Table 3. These response quantities when compared with existing results by Dyke et al. (1996) shows very good agreement (difference is ~5%).

Seismic response quantities for controlled modal building are evaluated using proposed instantaneous damping approach and constant damping approach and are compared with uncontrolled modal building in Table 3 for El Centro seismic excitations. Performance of passive SMA-TSD is compared with magneto-rheological (MR) fluid damper-passive off case with constant applied voltage of 2.5 V, as seismic response quantities for controlled modal building with this case were reported by Dyke et al. (1996). It is evident from Table 3 that SMA-TSD with constant damping approach yields substantial reduction (> 44%) in peak displacement, interstory and acceleration response quantities vis-à-vis uncontrolled modal building. Reduction in these response quantities is found to be moderate (13%–22%) for controlled modal building with instantaneous damping approach. Comparison amongst seismic response quantities for controlled modal building with passive SMA-TSD (constant damping approach) and with MR

damper passive off case shows comparable reduction with maximum difference of ~17%. Thus, passive SMA-TSD (constant damping approach) proves to be as effective as MR damper passive off case as observed in Table 3. Similar or better seismic response control of modal building with SMA-TSD can be obtained by adjusting design parameters; diameter and length of NiTinol wires, other than the ones used in the present study given in Table 4.

Peak seismic response quantities for controlled modal building subjected to seismic excitations have been determined. In this section, representative plots of Kobe seismic excitations – pulse type and El Centro seismic excitations – strong ground motion type are discussed. Peak displacement response of controlled modal building subjected to Kobe and El Centro seismic excitations are plotted in Figure 5(a) and Figure 5(b). It is evident that peak displacement reduces substantially at each story of the modal building. Peak displacement at roof level shows reduction of 47.96% for controlled building with constant damping approach under El Centro seismic excitations. It is seen that SMA-TSD with constant damping approach yields maximum reduction in seismic response quantities followed by instantaneous damping approach vis-à-vis uncontrolled modal building.

**Figure 5** Peak displacement response of controlled modal building to seismic excitations; (a) Kobe and (b) El Centro

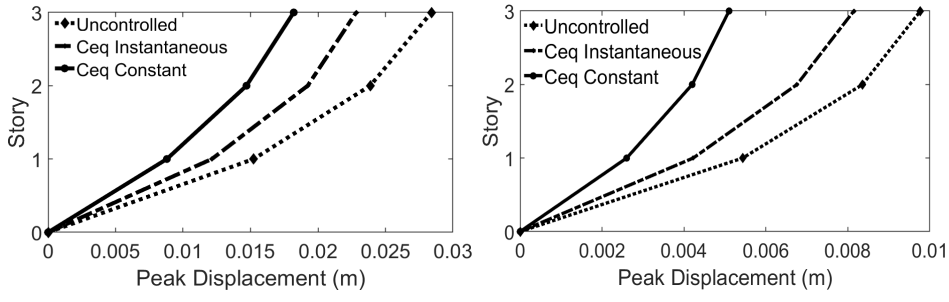


(a) (b)

Figure 6(a) and Figure 6(b) shows peak interstory drift response for controlled modal building showing maximum interstory drift occurring at first story level. SMA-TSD with both, instantaneous and constant damping yields reduction in peak interstory drift for each story of the modal building. While instantaneous damping approach brings similar order reduction, in peak interstory drift at each story of modal building under both Kobe and El Centro seismic excitation, constant damping approach yields relatively higher reduction in peak interstory drift for El Centro seismic excitation than the Kobe seismic excitation. Maximum attenuation in peak interstory drift is found to be 51.85% at first story of controlled modal building with constant damping approach under El Centro seismic excitations. Reduction in peak interstory drift at first story of controlled modal building is 22.22% under Taft seismic excitation which is least amongst all seismic excitations considered for the study. SMA-TSD with constant damping approach performs better than practical instantaneous damping approach due to higher stiffness and damping values which remain constant over seismic excitation events.

**Table 3** Peak seismic response quantities for three story modal building for El Centro seismic excitations

| | Story level | Uncontrolled response | | Controlled response | | |
|---|---|---|---|---|---|---|
| | | | | | Passive SMA-TSD | |
| | | Dyke et al. | Present study | MR damper passive off case Dyke et al. | Instantaneous damping approach (present study) | Constant damping approach (present study) |
| Peak displacement (cm) | 1 | 0.54 | 0.54 | 0.21 | 0.42 | 0.26 |
| | | | (0.00) | (–60.78) | (–22.22) | (–51.85) |
| | 2 | 0.82 | 0.84 | 0.36 | 0.68 | 0.42 |
| | | | (2.44) | (–56.46) | (–19.05) | (–50.00) |
| | 3 | 0.96 | 0.98 | 0.46 | 0.81 | 0.51 |
| | | | (2.00) | (–52.70) | (–17.35) | (–47.96) |
| Peak inter–story drift (cm) | 1 | 0.54 | 0.54 | 0.21 | 0.42 | 0.26 |
| | | | (0.37) | (–60.78) | (–22.22) | (–51.85) |
| | 2 | 0.32 | 0.30 | 0.15 | 0.26 | 0.16 |
| | | | (–6.33) | (–52.04) | (–13.33) | (–46.67) |
| | 3 | 0.20 | 0.19 | 0.10 | 0.16 | 0.10 |
| | | | (–5.47) | (–48.76) | (–15.79) | (–47.37) |
| Peak acceleration ($m/s^2$) | 1 | 8.56 | 8.38 | 4.20 | 6.60 | 4.64 |
| | | | (–2.18) | (–50.93) | (–21.24) | (–44.65) |
| | 2 | 10.30 | 10.69 | 4.80 | 8.45 | 5.54 |
| | | | (3.75) | (–53.40) | (–20.89) | (–48.12) |
| | 3 | 14.00 | 13.48 | 7.17 | 10.69 | 6.90 |
| | | | (3.87) | (–48.79) | (–20.72) | (–48.84) |
| Damper force (N) | | | | 258.00 | 116.14 | 79.16 |

**Figure 6** Peak interstory drift response of controlled modal building to seismic excitations; (a) Kobe and (b) El Centro

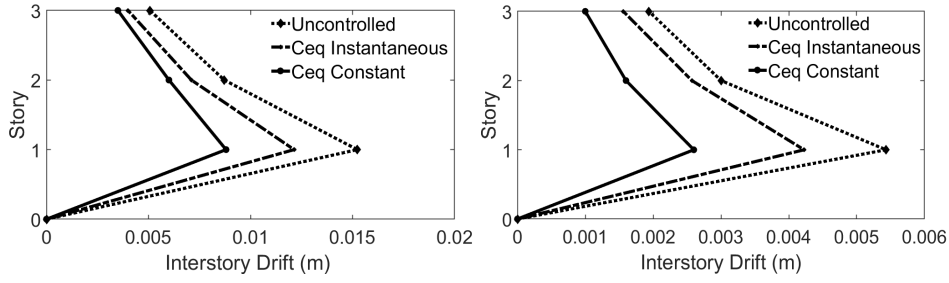


(a) (b)

Peak acceleration response of controlled modal building under Kobe and El Centro seismic excitations is plotted in Figure 7(a) and Figure 7(b), respectively. It is evident that SMA-TSD with both instantaneous and constant damping approach yields substantial reduction at each story of the modal building. Roof peak acceleration reduces to 20.72% and 48.84% for controlled modal building with instantaneous and constant damping approach, respectively, under El Centro seismic excitation. It is observed that similar to peak interstory drift response quantity, SMA-TSD with constant damping approach yields substantial reduction in peak acceleration response quantity at each story for El Centro seismic excitation. It is seen that amongst all seismic excitations considered, reduction in peak acceleration response quantity at each story is least for Taft seismic excitation.

**Figure 7** Peak acceleration response of controlled modal building to seismic excitations; (a) Kobe and (b) El Centro

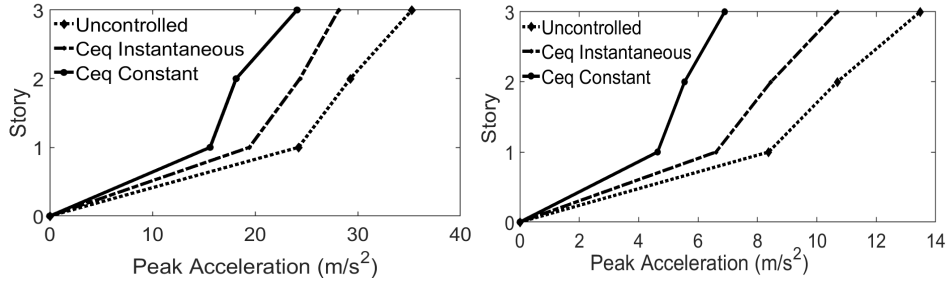


(a) (b)

Controlled modal building with both instantaneous and constant damping approach yields moderate to substantial reduction in all seismic response quantities under pulse type as well as strong motion type seismic excitations considered for the present study. It has been found that SMA-TSD with constant damping approach yields higher reduction in all seismic response quantities than one with instantaneous damping approach. This is attributed to maximum value assigned to stiffness and damping value for hysteretic SMA-TSD. It has been realised that seismic response of modal building can be controlled effectively if frequent phase transformation took place in SMA-TSD resulting into higher damping component of the Voigt model for SMA-TSD. Design parameters; numbers and

diameter of SMA tension slings are so adjusted that SMA-TSD with instantaneous damping approach act as stiffness device for strain values incapable of phase transformation under seismic excitations. This is true for substantial portion of seismic excitation data leading to limited damping contribution from SMA-TSD and is a major difference from constant damping approach. Thus, it is expected that seismic response of controlled modal building is relatively higher by instantaneous damping approach vis-à-vis constant damping approach. However, seismic response quantities show moderate reduction of response of controlled modal by instantaneous damping approach when compared with uncontrolled response of modal building.

**Figure 8** Roof displacement time history of controlled modal building to seismic excitations; (a) Kobe and (b) El Centro

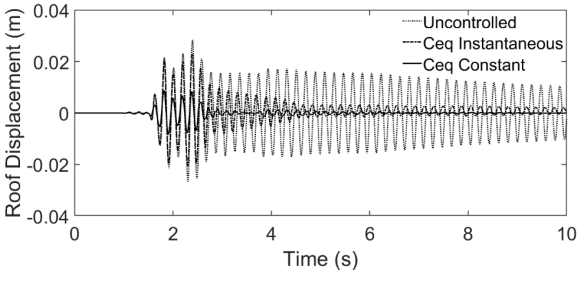


(a)

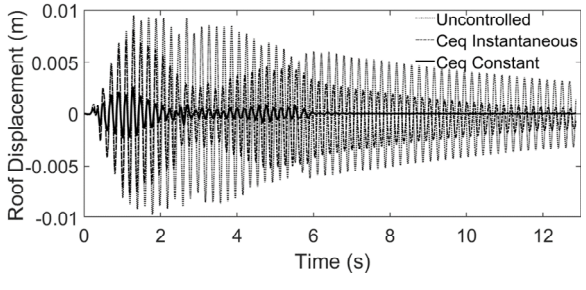


(b)

Roof displacement time history responses of controlled modal building subjected to Kobe and El Centro seismic excitations are shown in Figure 8(a) and Figure 8(b). It is clearly visible that passive SMA-TSD with both instantaneous damping and constant damping approach effectively control displacement response throughout seismic event. Similar displacement response results are obtained for controlled modal building for Lomaprieta and Taft seismic excitations. Uncontrolled peak roof displacement response of modal building 0.96 cm, reduces to 0.81cm (–17.35%) and 0.51 cm (–47.96%) for controlled modal building subjected to El Centro seismic excitation with instantaneous and constant damping approach, respectively. With instantaneous and constant damping approach, this quantity reduces from 0.79 cm to 0.70 cm (–11.39 %) and 0.34 cm (–56.96%) for Taft, from 1.85 cm to 1.18 cm (–36.46 %) and 1.07 cm (–42.16%) for Lomaprieta, from 2.84 cm to 2.28 cm ( –19.72 %) and 1.82 cm (–35.92%) for Kobe seismic excitations. It has been found that peak roof displacement for controlled modal building occurs earlier than uncontrolled modal building for all seismic excitations. It is also observed from

Figure 8(a) and Figure 8(b) that roof displacement of controlled modal building maintains static equilibrium position without any residual displacement from its base thus proving that strain in SMA-TSD remains within recoverable limits and design parameters of SMA are well placed.

**Figure 9** Roof acceleration time history of controlled modal building to seismic excitations; (a) Kobe and (b) El Centro

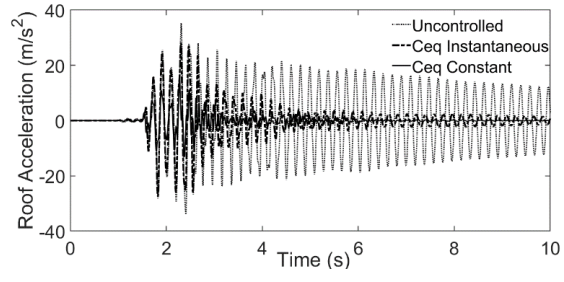


(a)

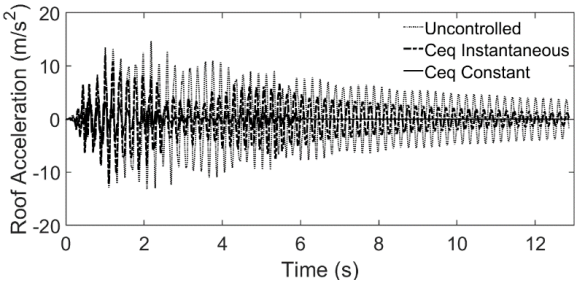


(b)

Figure 9(a) and Figure 9(b) represents roof acceleration time history response of controlled modal building under Kobe and El Centro seismic excitations. It is observed that passive SMA-TSD performs well to control roof acceleration of controlled modal building over entire seismic excitation event. Peak roof acceleration of uncontrolled building 14.00 m/s$^2$ reduces to 10.69 m/s$^2$ (20.72%) and 6.90 m/s$^2$ (48.84%) with instantaneous and constant damping approach, respectively, for El Centro seismic excitations. It is reduced from 9.193 m/s$^2$ to 8.093 m/s$^2$ (11.97%) and 4.065 m/s$^2$ (55.78%) for Taft, from 21.285 m/s$^2$ to 13.845 m/s$^2$ (34.95%) and 12.230 m/s$^2$ (42.54%) for Lomaprieta and from 35.283 m/s$^2$ to 28.146 m/s$^2$ (20.23%) and 24.088 m/s$^2$ (31.73%) for Kobe seismic excitations for instantaneous and constant damping approach, respectively. Similar to roof displacement time history responses, roof acceleration time history responses show early occurrence of peak value for controlled modal building vis-à-vis uncontrolled building. It can be seen from Figure 9(a) and Figure 9(b) that SMA-TSD with instantaneous damping approach shows relatively higher roof displacement and acceleration response as compared to constant damping approach for the reasons discussed earlier in the section.

Martensite Volume Fraction (MVF), as defined through equation (1) to equation (5), induced in SMA-TSD with instantaneous damping approach along with corresponding instantaneous damping ratio, as defined by equation (10), offered are plotted in

Figure 10(a) and Figure 10(b) for Kobe and El Centro seismic excitations. It is evident that, at each instant of time when SMA-TSD undergoes phase transformation indicated by MVF, equivalent viscous damping ratio sees increment in its value depending upon strain level present in the SMA-TSD. Thus, SMA-TSD offers additional stiffness and damping to the modal building during these time period results into reduction in seismic response quantities. For rest of the time period, when no phase transformation took place, SMA-TSD contributes additional stiffness to the modal building and thus acts as stiffness device only. It is observed that if design parameters are adjusted, SMA-TSD can contribute maximum additional damping of the order~ 20% to inherent damping of the modal building under various seismic excitations. However, numbers of time SMA-TSD undergoes phase transformation depends upon seismic input.

**Figure 10** Variation in martensite volume fraction and equivalent viscous damping ratio for SMA-TSD to seismic excitations, (a) Kobe and (b) El Centro

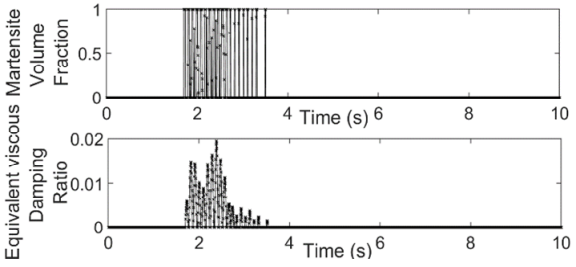


(a)

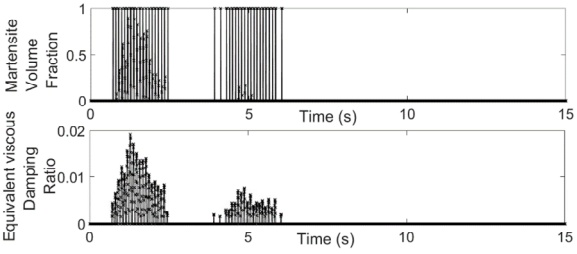


(b)

Damper force produced by passive SMA-TSD, $F_{SMA}$, with instantaneous and constant damping approach plotted in Figure 11(a) and Figure 11(b) for Kobe seismic excitations. Difference between these figures is width of hysteresis loop. Larger width of hysteresis loop obtained for SMA-TSD with constant damping approach is one to the fact that both stiffness and damping are added at each instant of time, irrespective of phase transformation. However, SMA-TSD with instantaneous damping approach adds only stiffness until strain in SMA-TSD reach to a limit of face transformation and thus, resulting into limited damping addition. This is evident as central portion of hysteresis loop is straight line with no width and thus, SMA-TSD behaves like a stiffness dependent device. Figure 12(a) and Figure 12(b) show damper force offered by passive SMA-TSD with instantaneous and constant damping approach for El Centro seismic excitations. A similar nature of damper force to displacement is observed for SMA-TSD to that of Figure 11(a) and Figure 11(b) with relatively lower stiffness but larger damping owing to

the seismic input. Peak damper force of 116.14 N and 74.16 N is achieved for SMA-TSD with instantaneous and constant damping approach, respectively. Table 4 shows peak-damper force offered by passive SMA-TSD under Lomaprieta and Taft seismic excitations. It is realised that use of prestraining action in action NiTi SMA wire for seismic application by Zhang and Zhu (2008) and some other research studies is justified in order to improve damping component of the SMA device. However, employing external means to improve damping component of SMA device are in developing phase.

**Figure 11** Damper force vs displacement for SMA-TSD to Kobe seismic excitations using (a) instantaneous damping approach (b) constant damping approach

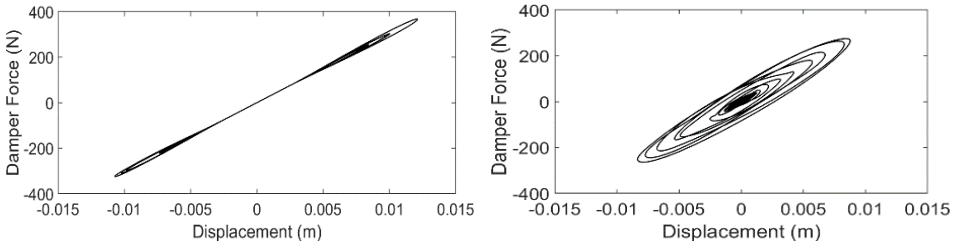


(a) (b)

**Figure 12** Damper force vs. displacement for SMA-TSD to El Centro seismic excitations using (a) instantaneous damping approach (b) constant damping approach

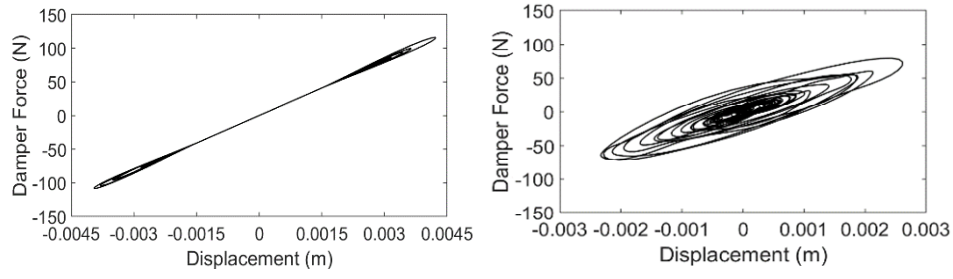


(a) (b)

Normalised performance indices (PI) are defined by equation (16) in Section 3 are determined for controlled modal building subjected to pulse and strong motion type seismic excitations given in Table 2. Design parameters; numbers, diameter and length of SMA sling are evaluated through iterative process such that it yields reduction in seismic response quantities. In the present study design iterations were carried out keeping diameter of SMA sling as 0.58 mm since mechanical properties were derived for this diameter in experimental studies by Zhang and Zhu (2008) and numbers of tension slings as 1, in order to study performance of SMA-TSD under different seismic excitations. Table 4 summarises PI's along with maximum strain in damper and peak-damper force for pulse and strong motion type seismic excitations. It is evident that passive SMA-TSD performs well and substantially reduces all PI's barring few of them where reduction is moderate under all seismic excitations. Passive SMA-TSD requires relatively higher tension sling length to achieve seismic response control of modal building when subjected to pulse type seismic excitations as compared to strong motion type seismic

excitations. This may cause some practical difficulties in installation of SMA-TSD with modal building. However, design parameters of passive SMA-TSD can be adjusted to fit in with requirements. Base shear PI, $J_3$ reduces substantially as SMA-TSD increases damping over inherent damping of the modal building. Control force PI, $J_{11}$ indicates that with relatively low control efforts from SMA-TSD, substantial reduction in seismic response quantities of modal building is achieved.

**Table 4** Seismic response performance indices for controlled modal building

| *Seismic excitations* | *SMA sling length (m)* | *Modelling approach (1*, 2*)* | *Performance indices (PI)* | | | | *Maximum strain in damper* | *Peak damper force (N)* |
|---|---|---|---|---|---|---|---|---|
| | | | $J_1$ | $J_2$ | $J_3$ | $J_{11}$ | | |
| Kobe | 0.50 | 1 | 0.797 | 0.798 | 0.350 | 0.127 | 0.022 | 275.34 |
| | | 2 | 0.578 | 0.675 | 0.182 | 0.095 | 0.018 | 368.89 |
| Loma-prieta | 0.4 | 1 | 0.623 | 0.650 | 0.581 | 0.051 | 0.014 | 145.97 |
| | | 2 | 0.618 | 0.604 | 0.312 | 0.049 | 0.014 | 141.57 |
| El Centro | 0.26 | 1 | 0.778 | 0.793 | 0.542 | 0.040 | 0.015 | 116.14 |
| | | 2 | 0.486 | 0.521 | 0.148 | 0.027 | 0.010 | 79.16 |
| Taft | 0.185 | 1 | 0.903 | 0.784 | 0.539 | 0.003 | 0.009 | 7.51 |
| | | 2 | 0.778 | 0.766 | 0.374 | 0.003 | 0.009 | 8.21 |

Note: 1*-Instantaneous damping approach, 2*-Constant damping approach.

It is observed that from Table 4 that maximum strain produced in SMA-TSD is within~ 2.5% under each type of excitations considered in this study. SMA-TSD with instantaneous damping approach yields higher or equivalent maximum strain vis-à-vis constant damping approach. Difference in maximum strain is 22.22% and 50% for Kobe and El Centro seismic excitations, respectively. Passive SMA-TSD undergoes higher maximum strain when subjected to pulse type seismic excitations.

## 5 Conclusions

NiTi based SMA is used to produce damper force from novel SMA-TSD fitted at ground story of the modal building by Dyke et al. (1996), subjected to pulse type and strong motion type seismic excitations. One-dimensional Tanaka model is considered to represent hysteretic behaviour of SMA-TSD due to its versatility. Characterisation of SMA-TSD under seismic excitations are carried out using linear Voigt model to map non-linear hysteretic behaviour of Tanaka model following AASHTO guide specifications for seismic isolation design. Linear Voigt model comprising of equivalent stiffness and damping components is implemented with linear modal building using practical instantaneous damping approach featured in the present study and constant damping approach used in other research studies. Seismic response quantities; peak displacement, interstory drift, acceleration, normalised PI, maximum strain, and damper force are evaluated for uncontrolled and controlled modal building under seismic excitations. Design iterations are performed for SMA-TSD design parameters; diameter, length and number of tension slings to achieve seismic response control of modal building.

Following conclusions are made from the present study:

1 Proposed superelastic SMA-TSD reduces seismic response quantities moderately (~13%–23%) with instantaneous damping approach and substantially (~44%–52%) with constant damping approach for controlled modal building.

2 Proposed SMA-TSD with constant damping approach performs at par with MR damper – passive off case of Dyke et al. for controlled modal building subjected to El Centro seismic excitations.

3 Design parameters of SMA-TSD are so adjusted that maximum strain induced in SMA tension sling under various seismic excitations remain within ~3% (< 4.5% of elastic recoverable strain) making it purely super elastic device effective in seismic response control of modal building without residual displacement.

4 Normalised performance indices (PI), peak inter story drift $J_1$, level acceleration $J_2$, base shear $J_3$ and control force $J_{11}$ show moderate to substantial reduction for controlled modal building fitted with SMA-TSD under pulse and strong motion type seismic excitations considered in the present study.

5 Passive SMA-TSD requires relatively larger sling length for seismic control of modal building under pulse type seismic excitations as compared to strong motion type seismic excitation.

6 Passive SMA-TSD with 0.58 mm diameter and single tension sling of varied length adds supplemental damping of the order 1.9%–20.6% to the controlled modal building under various seismic excitations

7 Representation of hysteresis behaviour with linear Voigt model seems to be justified as maximum damping ratio achieved by passive SMA-TSD for various seismic excitation is of the order ~21% is lower than permissible limit of 30%, damping ratio representing linear viscous damping for hysteretic device, defined by AASHTO guide specifications for seismic isolation design.

Installation of SMA-TSD with modal building may require careful attention when designed length of SMA slings are relatively longer with respect to story dimensions. Another set of design parameters for SMA-TSD which can yield similar or better seismic response control of modal building than the present study may be arrived using various optimisation techniques with constraint function on displacement and/or acceleration response.

## References

AASHTO (2014) *Guide Specifications for Seismic Isolation Design*, 4th ed., American Association of State Highways and Transportation Officials, Washington, DC.

Brinson, L.C. (1993) 'One dimensional constitutive behavior of shape memory alloys: thermomechanical derivation with non-constant material functions', *Journal of Intelligent Material Systems and Structures*, Vol. 4, No. 2, pp.229–242.

Buehler, W. and Wiley, R. (1961) *Nickel Based Alloys*, patent US3174851A.

Clarke, P.W., Aiken, I.D., Kelly, J.M., Higashino, M. and Krumme R. (1995) 'Experimental and analytical studies of shape-memory alloy dampers for structural control', *Proceedings of SPIE*, San Diego, CA, US, Vol. 2445, pp.241–251.

Dasgupta R. (2014) 'A look into Cu-based shape memory alloys: present scenario and future prospects', *Journal of Materials and Research*, Vol. 29, No.16, pp. 1681-1698.

Dolce, M., Cardone, D., Ponzo, F. and Valente, C. (2005) 'Shaking table tests on reinforced concrete frames without and with passive control systems', *Earthquake Engineering and Structural Dynamics*, Vol. 34, No. 14, pp.1687–1717.

Dyke, S.J., Spencer, B.F. Jr., Sain, M.K. and Carlson, J.D. (1996) 'Modelling and control of magnetorheological dampers for seismic response reduction', *Smart Materials and Structures*, Vol. 5, No. 5, pp.565–575.

Fan, Y., Sun, K., Zhao, Y., Yu, B. and Fan Y. (2019) 'A simplified constitutive model of Ti-Ni SMA with loading rate', *Journal of Materials Research and Technology*, Vol. 8, No. 6, pp.5374–5383.

Foti D. (2014) 'Response of frames seismically protected with passive systems in near-field areas', *International Journal of Structural Engineering*, Vol. 5, No. 4, pp.326–345.

Ghodke, S. and Jangid, S. (2016) 'Equivalent linear elastic-viscous model of shape memory alloy for isolated structures', *Advances in Engineering Software*, Vol. 99, No. 22, pp.1–8.

Graesser, E. and Cozzarelli, F. (1991) 'Shape-memory alloys as new materials for seismic isolation', *Journal of Engineering Mechanics*, Vol. 117, No. 11, pp.2590–608.

Hartl, D.J. and Lagoudas, D.C. (Eds.) (2008) *Thermomechanical Characterization of Shape Memory Alloy Material, Shape Memory Alloys: Modelling and Engineering Applications*, pp.53–119, Springer Science, ISBN: 978-1-4419-4297-5.

Huang, B., Zhang, H., Wang, H. and Song, G. (2014) 'Passive base isolation with superelastic NiTinol SMA helical springs', *Smart Materials and Structures*, Vol. 23, No. 6, 065009.

Jani, J.M., Leary M., Subic A. and Gibson, M.A. (2014) 'A review of shape memory alloy research, applications and opportunities', *Materials and Design*, Vol. 54, pp.1078–1113.

Jansen, L.M. and Dyke, S.J. (1999) 'Semi-active control strategies for MR dampers: a comparative study', *Journal of Engineering Mechanics*, Vol. 126, No. 8, pp.795–803.

Lavasani, S.H.H. and Doroudi, R. (2020) 'Meta heuristic active and semi-active control systems of high-rise building', *International Journal of Structural Engineering*, Vol. 10, No. 3, pp.232–253.

Liang, C. and Rogers, C.A. (1997) 'One-dimensional thermomechanical constitutive relations for shape memory materials', *Journal of Intelligent Material Systems and Structures*, Vol. 8, No. 4, pp.285–302.

Mans, M.D., Charney, F.A., Whittaker, A.S., Constantinou, M.C., Kircher, C.A., Johnson, M.W. and McNamara, R.J. (2008) 'Energy dissipation systems for seismic applications: current practice and recent developments', *Journal of Structural Engineering*, Vol. 134, No. 1, pp.4–21.

McCormik, J., DesRoches, R., Fugazza, D. and Auricchio, F. (2006) 'Seismic vibration control using superelastic shape memory alloys', *Journal of Engineering Materials and Technology*, Vol. 128, No. 3, pp.294–301.

Miller, D.J., Fahnestock, L. and Eatherton, M. (2012) 'Development and experimental validation of a Nickel – Titanium shape memory alloy self centering and buckling restrained braces', *Engineering Structures*, Vol. 40, pp.288–298.

Mortazavi, S.M.R., Ghassemieh, M. and Motahari, S.A. (2013) 'Seismic control of steel structures with shape memory alloys', *International Journal of Automation and Control Engineering*, Vol. 2, No. 1, pp.28–34.

Ocel, J., DesRoches, R., Leon, R., Gregory Hess, W., Krumme, R., Hayse, J.R. and Sweeney, S. (2004) 'Steel beam-column connections using shape memory alloys', *Journal of Structural Engineering*, Vol. 130, No. 5, pp.732–740.

Ohtori, Y., Christensen, R.E., Spencer, B.F. Jr. and Dyke, S.J. (2004) 'Benchmark problems for seismically excited nonlinear buildings', *Journal of Engineering Mechanics*, Vol. 103, No. 4, pp.366–385.

Ozdemir, H. (1976) *Nonlinear Transient Dynamic Analysis of Yielding Structures*, PhD Dissertation, University of California at Berkeley, Berkeley, CA.

Purohit, S.P. and Chandiramani, N.K. (2010) 'Optimal static output feedback control of a building using an MR damper', *Structural Control and Health Monitoring*, Vol. 18, No. 8, pp.852–868.

Ren, W., Hongnan, L. and Gangbing S. (2007) 'A one-dimensional strain-rate-dependent constitutive model for superelastic shape memory alloys', *Smart Materials and Structures*, Vol. 16, No. 1, pp.191–197.

Sodha, A.H., Soni, D.P. and Vasanwala, S.A. (2021) 'Evaluation of linear viscoelastic model of quintuple friction pendulum isolator', *International Journal of Structural Engineering*, Vol. 11, No. 1, pp.19–43.

Song, G., Ma, N. and Li, H.N. (2006) 'Applications of shape memory alloys in civil structures', *Engineering Structures*, Vol. 28, No. 9, pp.1266–1274.

Soong, T.T. and Constantinou M.C. (1994) *Passive and Active Vibration Control in Civil Engineering*, pp.271–274, Springer Science, ISBN: 978-3-211-82615-7.

Soong, T.T. and Spencer B.F. (2002) 'Supplementary energy dissipation: state-of-the-art and state-of-the-practice', *Engineering Structures*, Vol. 24, No. 3, pp.243– 259.

Spencer, B.F. and Nagarajaiah, S. (2003) 'State of the art structural control', *Journal of Structural Engineering*, Vol. 129, No. 7, pp.845–856.

Sun, C.T. and Lu, Y.P. (1995) *Vibration Damping of Structural Elements*, Prentice Hall Series, Pearson Publications, ISBN 0130792292.

Tanaka, K. (1986) 'A thermomechanical sketch of shape memory effect: one-dimensional tensile behaviour', *Research Mechanical*, Vol. 2, No. 3, pp.59–72.

Tobushi, H., Shimeno, Y., Hachisuka, T. and Tanaka, K. (1998) 'Influence of strain rate on superelastic properties of TiNi shape memory alloy', *Mechanics of Materials*, Vol. 30, No. 2, pp.141–150.

Tsai, H.C. and Kelly, J.M. (1994) 'Seismic response of heavily damped base isolation systems', *Earthquake Engineering and Structural Dynamics*, Vol. 22, No. 7, pp.633–645.

Wilde, K., Gardoni P. and Fujino Y. (1998) 'Experimental and analytical study on a shape memory alloy damper', *Smart Structures and Materials 1998: Smart Systems for Bridges, Structures and Highways Proc. SPIE*, San Diego, CA, US, Vol. 3325, pp.182–191.

Xu, Y.L., Qu, W.L. and Ko, J.M. (2000) 'Seismic response control of frame structures 'using magnetorheological/electrorheological dampers', *Earthquake Engineering Structural Dynamics*, Vol. 29, No. 5, pp.557–575.

Zhang, Y. and Zhu, S. (2007) 'A shape memory alloy-based reusable hysteretic damper for seismic hazard Mitigation', *Smart Materials and Structures*, Vol. 16, No. 5, pp.1603–1613.

Zhang, Y. and Zhu, S. (2008) 'Seismic response control of building structures with superelastic shape memory alloy wire dampers', *Journal of Engineering Mechanics*, Vol. 134, No. 3, pp.240–251.